

# BEHAVIORAL AND NEURAL VARIABILITY OF NATURALISTIC ARM MOVEMENTS

Steven M. Peterson<sup>1,2\*</sup>, Satpreet H. Singh<sup>3\*</sup>, Nancy X. R. Wang<sup>4,5</sup>, Rajesh P. N. Rao<sup>3,5,6</sup>, Bingni W. Brunton<sup>1,2†</sup>

<sup>1</sup>Department of Biology, University of Washington, Seattle, WA 98195, USA

<sup>2</sup>eScience Institute, University of Washington

<sup>3</sup>Department of Electrical and Computer Engineering, University of Washington

<sup>4</sup>IBM Research, San Jose, CA 95120, USA

<sup>5</sup>Paul G. Allen School of Computer Science and Engineering, University of Washington

<sup>6</sup>Center for Neurotechnology, University of Washington

## ABSTRACT

Motor behaviors are central to many functions and dysfunctions of the brain, and understanding their neural basis has consequently been a major focus in neuroscience. However, most studies of motor behaviors have been restricted to artificial, repetitive paradigms, far removed from natural movements performed “in the wild.” Here, we leveraged recent advances in machine learning and computer vision to analyze intracranial recordings from 12 human subjects during thousands of spontaneous arm reach movements, observed over several days for each subject. These naturalistic movements elicited cortical spectral power patterns consistent with findings from controlled paradigms, but with an important difference: there was considerable neural variability across subjects and events. We modeled inter-event variability using ten behavioral and environmental features; the most important features explaining this variability were reach angle and recording day. Our work is among the first studies connecting behavioral and neural variability across cortex in humans during spontaneous movements and contributes to our understanding of long-term naturalistic behavior.

Natural human movements are remarkable in their complexity and adaptability, relying on precisely coordinated sensorimotor processing in several cortical regions [1–4]. Much of our understanding on the neural basis of movement has been gained by studying constrained, repetitive movements in the laboratory, but it remains unclear how well these results generalize to the spontaneous actions observed in the real world [5]. Focusing on more naturalistic behaviors enriches our understanding of the relationship between motor behavior and cortical activation [6–8]. Further, these data and insights motivate development of more robust brain-computer interfaces to restore impaired movement and sensation across diverse contexts [9–13].

The history of modern neuroscience has seen a consistent trend towards studies incorporating more naturalistic elements. The use of stimuli, environments, and tasks with increasing ecological relevance to the animal has enhanced our understanding of how the brain functions, complementing results from more artificial laboratory paradigms. For instance, early neural recordings focused on anesthetized animals, but the transition to experiments with awake, behaving animals transformed our knowledge of sensory, motor, and cognitive brain functions [14–18]. More recently, researchers have moved towards using natural auditory and visual stimuli, finding novel neural responses not seen with artificial stimuli [19–24]; moreover, features of natural stimuli often better explain the observed variance in neural activity [25, 26]. In human neuroscience and behavior, advances in technology have enabled an expanded focus on a variety of mobile outdoor paradigms [27–31], spatial navigation tasks within immersive virtual environments [32, 33], and tasks involving active social interactions [34–37].

Intracranial electrophysiological recordings offer a unique view into the neural correlates of human behavior. These recordings, obtained using electrocorticography (ECoG), contain physio-

logically relevant spectral power patterns corresponding to a variety of behaviors [38–42]. ECoG recording electrodes are implanted on the cortical surface, beneath the skull and dura; these signals are thus cleaner and less susceptible to artifact contamination than signals from electroencephalography (EEG) [43]. Although implanting ECoG electrodes is an invasive neurosurgical procedure, the recordings are highly informative and have a combination of high spatial and temporal resolution not found in other commonly used human neuroimaging or neural recording modalities [44–46]. During instructed upper limb movements, ECoG spectral power in fronto-parietal cortical areas, particularly over sensorimotor cortex, has been shown to transiently increase at high frequencies and decrease at low frequencies [4, 47, 48]. Similar spectral power changes have been observed in EEG and local field potential recordings across a wide variety of movement behaviors [49–53]. An important attribute of ECoG recordings is that the patients are being continuously monitored over long periods of time, often approximately a week, providing unique opportunities to collect long-term datasets during unconstrained, uninstructed movements [54–59]. The behavioral and neural variability of such spontaneous, naturalistic movements have remained unexplored.

Analyzing naturalistic data presents formidable challenges, but recent innovations in data science make it possible to extract meaningful findings from increasingly complex, including naturalistic and opportunistic, datasets [62]. Without prior experimental design or direct behavioral measurements, a critical first step in analyzing naturalistic data had previously been laborious manual annotation of behavior. Such tedious labeling severely limits the amount of usable data and is prone to subjective error. Fortunately, recent advances in computer vision and machine learning have enabled substantial automation of the analysis and quantification of naturalistic behaviors [60, 63–66].

\* Contributed equally

† Correspondence: stepeter@uw.edu and bbrunton@uw.edu

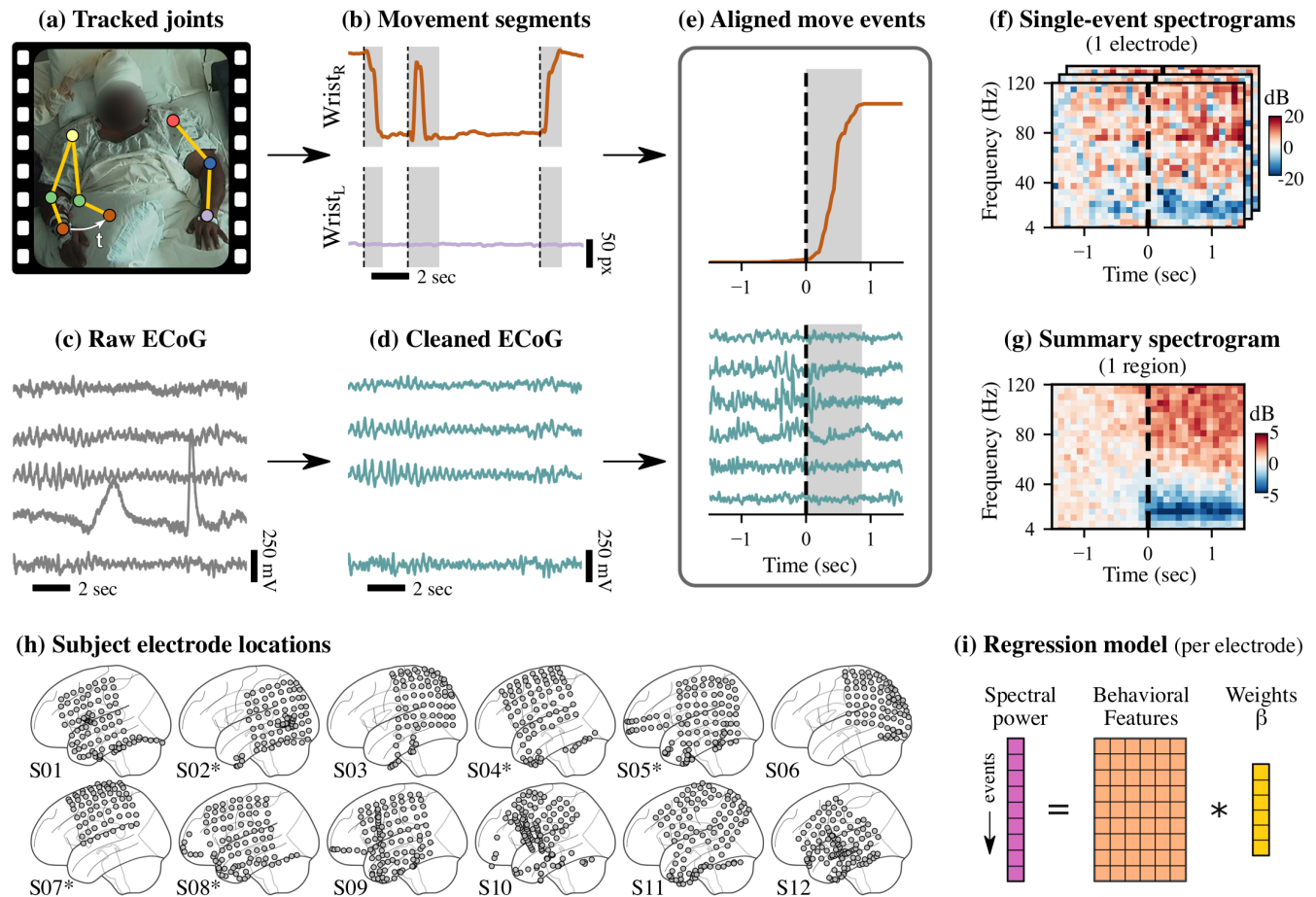


**Fig. 1: Schematic overview of data processing, analysis, and modeling framework.** (a)–(b) Based on continuous video monitoring of each subject, trajectories of the left and right wrists (Wrist<sub>L</sub> and Wrist<sub>R</sub> in (b)) were estimated using neural networks [60] and automatically segmented into move (gray) and rest (white) states as shown in (b) [61]. (c)–(d) Raw multi-electrode electrocorticography (ECoG) was filtered and re-referenced; bad electrodes (e.g., ones with artifacts) were removed from further analysis. (e) Movement onset events detected from video as shown in (b) were aligned with ECoG data using timestamps. (f) For each move event at each electrode, spectral power was computed and visualized as a log-scaled spectrogram. (g) Summarizing across events and electrodes, we projected the spectral power from electrodes onto 8 cortical regions based on anatomical registration and computed the median power across movement events. (h) Our data included 12 subjects; their electrode placements are shown in MNI coordinates. Five of the subjects had electrodes implanted in their right hemispheres (denoted by asterisks). For consistency of later analyses, we mirrored the locations of these electrodes as shown here. (i) To partially explain the event-by-event neural variability, we fit multiple linear regression models at each electrode using behavioral features extracted from the videos.

Even so, making sense of the recorded behaviors remains challenging in the absence of a rigid, trial-based structure. Behavioral and neural variables are often continuous valued, not discrete, and the complex interactions of multiple variables make it difficult to compare averaged data across conditions [67]. One widely used approach to address this problem is the use of regression models. These models attempt to explain neural variability via regression using behavioral and environmental input features and have been effectively employed across many behavioral paradigms and neural recording modalities [68–71].

In this paper, we analyzed opportunistic, clinical intracranial recordings from 12 human subjects across 3–5 days each as we observed their naturalistic spontaneous arm movements. We developed an automated approach to identify and characterize thousands of spontaneous arm movements, enabling scalable analysis of video that was acquired simultaneously with the intracranial recordings. We characterized the variability of both naturalistic upper-limb reaching movements and the corresponding changes in cortical spectral power. Based on findings from controlled experiments, we hypothesized that naturalistic reaches are associated with transient decreases in low-frequency power and increases in high-frequency power, localized to fronto-parietal sensorimotor cortices [4]. Our results support this hypothesis on average; however, we show that there is considerable natural variability in spectral power both within and across subjects. Next, we developed a multiple-variable linear regression model of the single-event spectral power variability based on 10 movement and environmental features, including reach angle, reach duration, day of recording, and presence of spoken words. We found that vertical reach angle and day of recording features best account for the observed neural variability across movement events, but much of the variance remains unexplained by the linear model. To support reproducibility and facilitate future research in naturalistic human movement analysis, we have made our curated dataset containing synchronized behavioral and neural data publicly available.

## RESULTS

We describe behavioral and neural variability observed in multi-electrode intracranial neural recordings and video obtained opportunistically from 12 human subjects during thousands of spontaneous arm movements. Each subject had been implanted with electrocorticography (ECoG) electrodes for clinical monitoring, and we analyzed 3–5 days of simultaneously recorded video and electrophysiological data following surgery. We developed an automated and scalable approach to tracking upper limb movements based on machine learning and then focused on analyzing spectral power changes associated with movements of the wrist contralateral to the hemisphere with electrode implantation (Fig. 1a–g). ECoG monitoring was clinically motivated, so there was substantial variation in electrode placement among subjects (Fig. 1h). Because our focus was on motor behaviors, we chose to analyze 12 subjects who were generally active during their monitoring and also had electrodes implanted over fronto-parietal sensorimotor cortical areas.

### *Naturalistic movements and intracortical spectral power*

The goal of our data processing pipeline was to automate both the robust identification of wrist movement initiation events

and the description of behavioral and environmental features around each event. For each subject, we obtained simultaneously recorded neural activity and movement trajectories immediately before and after the initiation of each movement event (Fig. 1e). Briefly, two-dimensional wrist trajectories were estimated from the video recordings [60] and then segmented into move or rest states [61]. For simplicity of interpretation, we focused on movement initiation events of the wrist contralateral to the ECoG implantation hemisphere, detected during transitions from rest to move states. Movements of primarily the ipsilateral arm and of both arms simultaneously are not considered in our analysis until the modeling described in a later section.

The spontaneous wrist movement events we identified include a wide variety of upper-limb movement behaviors. Because subjects were sitting in bed, a majority of the movements we analyzed involved relatively little movement of the shoulders and elbows (see, for example, Fig. 2a). Most of the detected movements corresponded to actions such as reaching for a phone, eating, or touching one's face. We find high variability in the contralateral wrist's 2D position and displacement following movement initiation (Fig. 2a–b). This large behavioral variability reiterates how spontaneous arm movements are distinct from instructed, repeated movements. Confirming that our event detection algorithm primarily identified contralateral wrist movements, the median contralateral wrist displacement across events notably increases during movement initiation compared to ipsilateral wrist displacement for all subjects (Fig. 2c).

We find a consistent set of group-level spectral power patterns, largely localized in fronto-parietal sensorimotor cortical regions. After aligning curated wrist movement events with preprocessed ECoG recordings, we computed time-frequency spectral power at each electrode and then visualized group-level spectral patterns projected onto common regions of interest for all subjects. Generally, we find the expected pattern of low-frequency (~4–30 Hz) spectral power decrease and high-frequency (~50–120 Hz) power increase during movement initiation across multiple cortices (Fig. 3), as reported in previous controlled movement experiments [4]. Because ECoG electrode placement varies across subjects, we visualize group-level neural activity by projecting power at every electrode onto 8 common cortical regions of interest [72]: middle frontal, precentral, postcentral, inferior parietal, supramarginal, superior temporal, middle temporal, and inferior temporal. Maximal power deviations primarily occur near movement onset, as expected. Spectral power deviations are largest in magnitude in precentral, postcentral, and inferior parietal regions, which are located in sensorimotor areas of the brain. The middle frontal region also contains strong power fluctuations that could indicate motor planning and possible recruitment of the supplementary motor area. In addition, low-frequency power decreases are more spatially widespread than high-frequency power increases, so they are also present in supramarginal and superior temporal regions. As expected, all 3 temporal cortical regions contain minimal movement-related spectral power fluctuations.

Despite these consistent group-level spectral power patterns across cortical regions, there is considerable spectral power variability across subjects (Supplementary Fig. 1). For instance, the postcentral region contains the same low/high-frequency

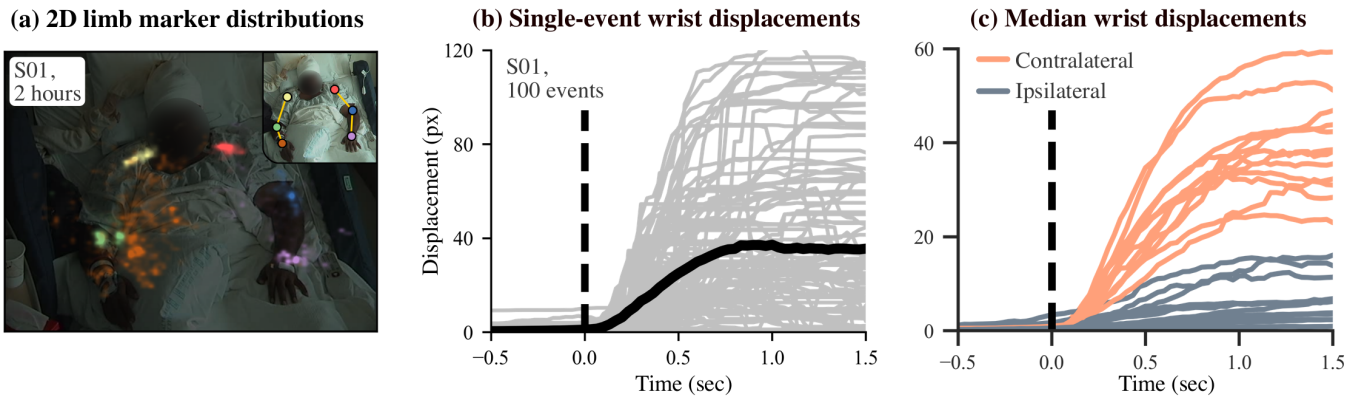


**Fig. 2: Behavioral variability during naturalistic movements is large.** (a) An example of tracked joint markers during 2 hours of video monitoring for S01. Movement events of S01's right wrist are visualized, as the subject's electrodes were implanted in the left hemisphere. A heatmap of locations of each joint is shown. (b) An example of 100 randomly selected movement trajectories of the right wrist for S01, shown as displacement in pixels from the rest position, demonstrates the large variability seen across naturalistic arm movements. Solid black line denotes median displacement across events. Events are aligned by time of movement initiation (vertical dashed line). (c) Because we selected movement initiation events of the wrist contralateral to the hemisphere with implanted electrodes, the median contralateral wrist displacements (orange lines) across all 12 subjects are substantially greater than ipsilateral wrist displacements (gray lines).

power pattern for each subject (Fig. 4), but the amplitudes and frequency bands of maximal power deviation differ widely across subjects. Subjects 03, 06, 07, 08, and 11 show increased power at high frequencies up to 120 Hz, while subjects 09 and 12 have increased power primarily between 60–80 Hz. For subjects 04 and 08, low-frequency power decreases occur across narrower frequency bands compared to the other subjects. Besides arising from inter-subject differences in neural anatomy and connectivity, these spectral power variations may reflect variability in daily activities, electrode placement, medication, and seizure foci among subjects [73, 74]. Spectral power plots for the 7 other regions of interest are shown in Supplementary Figs. 2–8.

#### Comparison of naturalistic movements to instructed hand clenches

For three of our subjects, we directly compared the neural correlates of naturalistic reaches with instructed movements during a controlled bedside experiment. We obtained ECoG and movement data during visually cued hand clenches in an experiment that had been performed with subjects 01–03 (as described in [75]). Hand movements were measured using a wired glove, which provided precise timing of hand clench initiation events. Each subject was instructed to clench their hand about 10 times, and the associated ECoG data was analyzed using the same time-frequency power methods applied to the naturalistic reaches (Fig. 1).

Both naturalistic reaches and experimental hand clenches show consistent median spectral power patterns in similar electrodes, but the behavioral and electrocortical variability is substantially higher during naturalistic reaches. For all 3 subjects, we find high standard deviations (SDs) for wrist displacement during naturalistic reaches, while the instructed hand clenches show less variation (Fig. 5a). This difference in SD across conditions is particularly striking because we compute the SD

with many more naturalistic reaches ( $484.0 \pm 241.1$  per subject [mean $\pm$ SD]) than instructed hand clenches ( $9.7 \pm 0.6$  per subject). Analyzing the neural data, we find that electrodes with significant power magnitudes in low/high-frequency bands (LFB/HFB) are mostly located in sensorimotor areas ( $p < 0.05$ , two-sided bootstrap statistics) (Fig. 5b). In both conditions, low-frequency power decreases appear spatially more widespread than high-frequency power increases, and time-frequency power patterns are visually similar (Supplementary Figs. 9 and 10). However, spectral power during naturalistic reaches shows decreased magnitude compared to instructed hand clenches. This decrease in power likely results from the significantly increased variability in LFB/HFB power compared to instructed hand clenches (Fig. 5c; LFB:  $W = 1009$ ,  $p = 1.8e-39$ , Pearson's  $r = 0.16$  and HFB:  $W = 7883$ ,  $p = 7.3e-14$ , Pearson's  $r = -0.07$ ; two-sided Wilcoxon signed-rank test).

#### Behavioral and environmental features of movement events

To explain the event-by-event variability in the spectral power at low and high frequency bands, we first extracted features of movement events and several associated environmental variables. We defined a *reach* as the maximum radial displacement of the wrist during the detected movement event, as compared to the wrist position at movement initiation. We extracted 10 behavioral metadata features that quantify the time when each reach began, how the contralateral wrist moved during the reach, whether people were speaking during movement initiation, and how much both wrists moved during each movement [61].

We found that many metadata feature distributions show large within-subject and between-subject variations (Fig. 6). The number of reaches detected across days of recording are fairly consistent, with the exceptions of subjects 04, 05, and 09, who each had one day representing most of the total events. As ex-

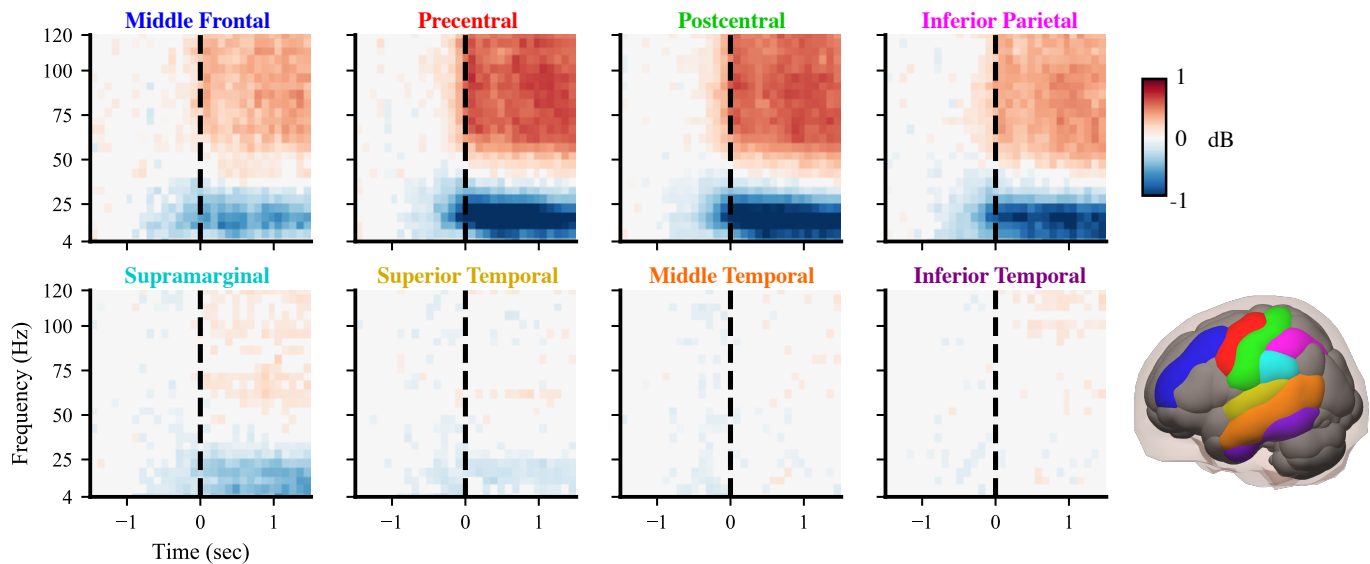


**Fig. 3: Group-level cortical spectral power changes are consistently localized to sensorimotor regions.** Spectrograms show movement event-triggered spectral power changes for 8 cortical regions (highlighted in lower right) summarized across all 12 subjects. On average, there are low-frequency (4–30 Hz) power decreases and high-frequency (50–120 Hz) power increases at time of movement initiation, with largest power fluctuations in fronto-parietal sensorimotor areas. Spectral power is projected based on anatomical registration from electrodes onto 8 regions of interest: middle frontal (blue), precentral (red), postcentral (green), inferior parietal (magenta), supramarginal (cyan), superior temporal (yellow), middle temporal (orange), and inferior temporal (purple). We subtracted the baseline power of 1.5–1 seconds before movement initiation. Non-significant differences from baseline power were set to 0 ( $p > 0.05$ ).

pected, detected movement events tend to have occurred mostly during waking hours. Reach duration and reach magnitude show less inter-subject variability, with most reaches lasting less than 2 seconds and covering less than 200 pixels (~67 cm). The distributions for reach angle tend to be bimodal, with peaks at  $\pm 90^\circ$ , indicating that detected events are biased towards upward and downward reaches, with few side-to-side reaches. Both onset speed and speech ratio distributions vary greatly across subjects, likely reflecting inter-subject differences in the activities performed and the number of people visiting during the detected movement initiations. We also considered a number of features related to coordinated movements that involve the ipsilateral arm. For bimanual ratio and overlap features, the distributions are skewed towards unimanual movements of the contralateral limb, as expected from Fig. 2c, with less skew for subjects 02, 04, and 05. In contrast, the bimanual class categorical feature is primarily skewed towards bimanual movements, indicating that the ipsilateral wrist is often moving, but only a small amount.

We also assess group-level correlations between feature pairs, finding high correlations for 3 reach parameter feature pairs and between all 3 bimanual feature pairs (Supplementary Fig. 11). Reach magnitude positively correlates with reach duration ( $r = 0.26$ ) and onset speed ( $r = 0.56$ ), meaning that reaches tend to cover more distance when they last longer or have higher onset speed. Reach duration is also positively correlated with bimanual overlap ( $r = 0.48$ ) due to movements with long duration having more possible overlap time. The high correlations between bimanual features (pairwise Pearson correlation coefficients between overlap v. ratio:  $r = 0.51$ , class v. ratio:  $r = 0.50$ , and overlap v. class:  $r = 0.61$ ) indicates that

contralateral wrist movements classified as bimanual generally show increased overlap between ipsilateral and contralateral movements and increased ipsilateral amplitude relative to contralateral, as expected.

#### Modeling single-event spectral power with behavioral features

We developed a robust multiple variable linear regression model to explain single-event spectral power at every intracranial electrode using our 10 behavioral metadata features (Fig. 1i). For each electrode, we chose to model the spectral power at two subject-specific frequency bands averaged over the half second following movement onset. The high- and low-frequency bands were chosen separately for each subject to acknowledge the large variability across subjects (high- and low-frequency bands for each subject are shown as dark and light gray bars in Fig. 4, respectively). For each model, behavioral features were pruned independently using forward selection to avoid overfitting. To assess each model, we randomly withheld 10% of movement events from training, then used this test data to compute the model's  $R^2$  performance (referred to as the *full model*  $R^2$ ). To assess the contributions of each individual feature, we shuffled all labels for that feature in the training data, fit a new linear model, and then computed this model's  $R^2$  on withheld data. We subtracted this new  $R^2$  from the full model  $R^2$  to obtain  $\Delta R^2$  as an estimate of feature importance. Higher  $\Delta R^2$  values indicate features that explain more variance.

Intracortical activity variability is best explained by our models fit to electrodes located in fronto-parietal sensorimotor areas (Fig. 7b). Of the many models fit across electrodes and frequency bands, we focus on well-fit models that have a positive

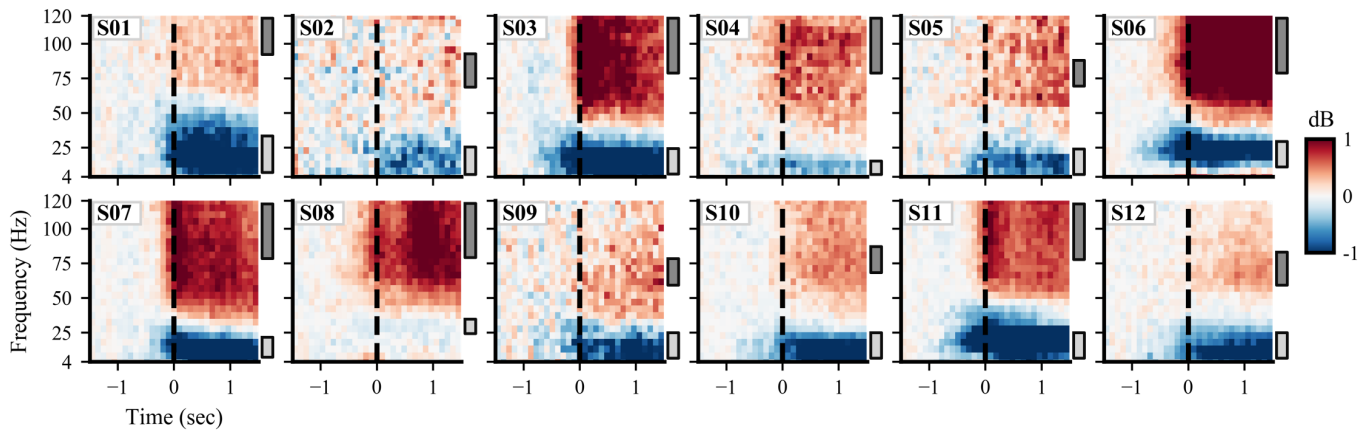


**Fig. 4: Spectral power patterns in the postcentral region of interest vary considerably across subjects.** Some subjects show spectral power patterns similar to the group-level results in Fig. 3, yet many deviate substantially from the expected pattern in both magnitude and frequency band of deviations from baseline. The colormap indicates differences in spectral power relative to baseline 1.5–1 seconds before movement initiation (no statistical masking is used). Boxes to the right of each panel indicate frequency bands with large positive (dark gray) and negative (light gray) deviations from baseline during the first half second following movement initiation. These subject-specific frequency bands were used to compute spectral power features used as targets in the multiple regression modeling.

$R^2$  on withheld data. While all but 1 subject had at least one well-fit model, the number of well-fit models per subject varies considerably, ranging from 1–29 (Fig. 7a). For both frequency bands, among the recorded cortical areas, the neural variability in sensorimotor areas was consistently best explained across all subjects, based on their relatively large full model  $R^2$  scores (Fig. 7b and Supplementary Fig. 12). This finding matches well with the spatial distribution of spectral power (see Fig. 3). We note that the maximum  $R^2$  is near 0.1, indicating that even the best models cannot explain ~90% of the variance in the withheld data. Among individual features, we find that reach angle and day of recording are the most informative (Fig. 7c). Interestingly, feature importance for day of recording appears more spatially localized than for reach angle, especially for the low frequency band. In addition to being informative, reach angle is also the most often retained feature following forward selection in sensorimotor regions (Supplementary Table 1), indicating its importance for modelling neural activity during movement onset.

In agreement with the  $R^2$  and  $\Delta R^2$  scores, both reach angle and day of recording have the largest coefficient magnitudes among behavioral features in the regression models (Fig. 8). The coefficients for these two features also show consistent magnitude and sign across subjects for electrodes located in sensorimotor areas. The coefficients for reach angle indicate that upward reaches are associated with decreased low frequency power and increased high frequency power compared to the average response. In other words, upward reaches tend to increase the magnitude of the spectral power pattern seen. In addition, we consider the day and time of day during which the movement was made. The SD of the coefficients corresponding to these timing features are large, indicating that neural responses vary across long time scales usually not captured in short, controlled experiments. This observation highlights the importance of properly accounting for long-term temporal effects when understanding and decoding neural recordings. These results mostly

match trends in the feature importance scores. Reach duration, reach magnitude, and onset speed have relatively large coefficients that are similar to the coefficients for reach angle, but these features may lack enough inter-event variability to provide useful predictions on withheld data. Note that the regression coefficients of all well-fit models are robust to the selection of train and test data, as seen in Supplementary Fig. 13.

## DISCUSSION

Our results demonstrate that electrocortical correlates of naturalistic arm movements in humans corroborate findings from controlled experiments on average, as we had hypothesized, but naturalistic movements exhibit high behavioral and neural variability. Using multiple regression modelling, we are able to partially explain this event-by-event electrocortical variability using behavioral metadata features extracted from video recordings. Of the 10 behavioral and environmental features used, vertical reach angle and day of recording account for most of the explained variance. Upward reaches are associated with increased cortical spectral power, and the significance of the day of recording feature highlights the importance of accounting for long-term neural variability.

Across subjects, we observe a consistent decrease in low-frequency band cortical power and increase in high-frequency band cortical power during naturalistic upper-limb movement initiation, consistent with previous controlled studies [4, 54]. Decreases in low-frequency power are thought to reflect changes in the current neural state if a new or unexpected event occurs [76]. In our study, the neural state can be disrupted during movement initiation by a variety of factors, such as increased attention or prediction error once the arm is in motion. In contrast, high-frequency power increases may indicate active sensorimotor processing [77–81]. Low-frequency and high-frequency power changes are thought to represent two separate processes [82, 83], which could explain the difference

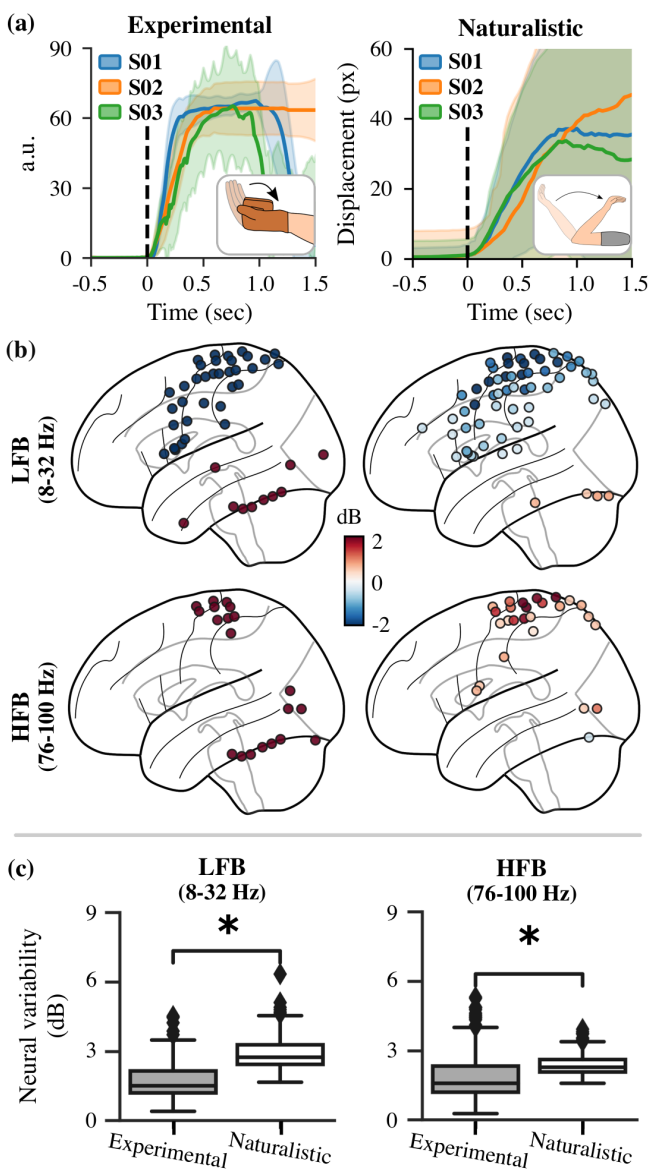


**Fig. 5: Naturalistic reaches are more variable than instructed hand clenches.** Movement initiation behaviors and the corresponding neural activity are shown for experimentally instructed hand clenches and naturalistic reaches for the same 3 subjects. (a) Median values for distal index joint voltage and wrist marker displacement are shown for hand clenches and reaches, respectively. Shaded standard deviation indicates increased behavioral variability during reaches compared to hand clenches. (b) For intracortical spectral power, we find similar low frequency band (LFB) and high frequency band (HFB) median power fluctuations across conditions for all 3 subjects during the first half second after movement initiation. Only electrodes with significant spectral power compared to baseline are shown ( $p < 0.05$ ). (c) For both LFB and HFB, neural variability was significantly increased during naturalistic reaches compared to experimentally instructed hand clenches ( $p < 0.05$ ). Variability was computed by the median absolute deviation of the spectral power for every electrode.

seen in the spatial spread of cortical power changes between low and high frequencies. Our regression analysis does not provide additional evidence for separate processes, as behavioral feature coefficients vary similarly across both frequency bands. However, the frequency bands of maximum spectral power responses do differ across subjects, which suggests that the processes underlying the low and high frequency bands vary across subjects. This inter-subject variability reinforces the importance of assessing both subject-specific neural responses and group-level activity.

Despite showing the expected cortical pattern on average, naturalistic reaches exhibited greater behavioral and neural variability than instructed hand clenches performed in a bedside experiment. Healthy human movements are often quite variable [84, 85], which has been shown to facilitate motor learning [86, 87]. The high variability seen during naturalistic reaches likely reflects variations in sensory input and movement constraints due to different types of behaviors [88]. In addition, the type of movement differs between conditions, which may explain some of the behavioral and neural variability that we observe. In particular, making a fist is a highly stereotyped movement, while reaching could invoke different muscle patterns depending on the direction moved. Even so, the naturalistic reaches contain higher neural and behavioral variability than instructed hand clenches, despite having ~36 times as many events per subject as the experimental clenches. Since the measures we use to estimate variability decrease as sample size increases, our results imply that naturalistic movements must contain high variability compared to instructed hand clenches. During modelling, we find that our models only explained at most ~10% of the variability; this measure is low, but not unusual given the single-event noise in the electrocortical signal. Further, some of this variability may be explained by other movement behaviors beyond what we quantified [89].

Our regression model identified vertical reach angle and day of recording as the most explanatory features. The importance of vertical reach angle is not surprising because upward reaches require more effort and activate different muscles than downward reaches. In addition, population neural activity has been shown to robustly encode reach direction [90, 91]. We did not include a reach angle feature sensitive to horizontal movements because reach angle distributions were skewed towards vertical angles at  $\pm 90^\circ$ , as seen in Fig. 6. The day of recording feature was also found to explain much of the variance captured by regression modelling. Neural variation across days of recording could be caused by several factors, including changes in medication, seizure frequency, and alertness while recovering from ECoG implantation surgery. Similar long-term, inter-day variability has been observed in previous EEG and ECoG studies [92–94]. It is also worth noting that these day-to-day changes in ECoG spectral power may be small; the average electrocortical response is only  $\pm 1\text{--}2$  dB. Furthermore, recent research suggests that despite long-term neural recording variability, low-dimensional representations of this activity remain stable over long periods of time [95].

Our study has several important limitations. First, we are studying subjects who have epilepsy and are recovering from electrode implantation surgery, which may introduce confounding effects due to medication and seizure location. To address this

## BEHAVIORAL & NEURAL VARIABILITY OF NATURALISTIC MOVEMENTS

8

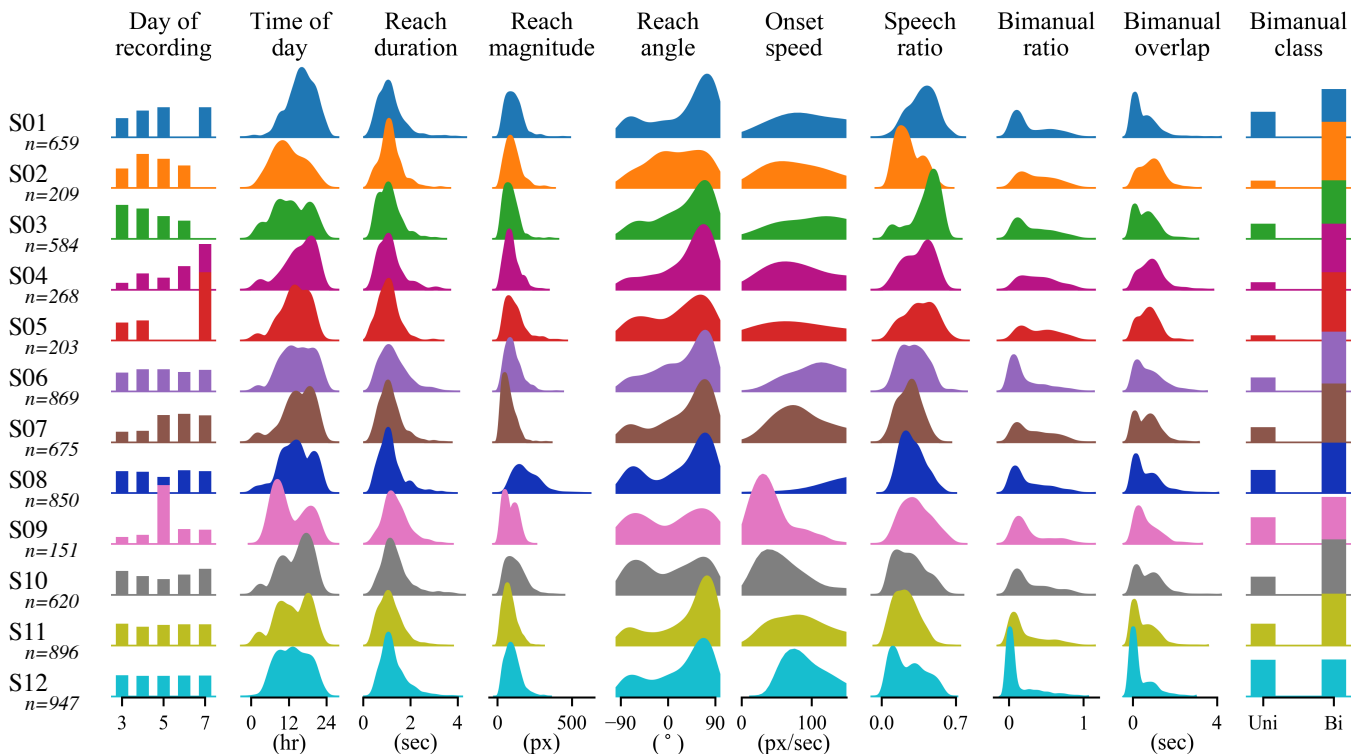


**Fig. 6: The distribution of extracted behavioral and environmental features show large inter-subject variability.** For each subject, features shown include timing (day of recording, time of day), reach parameters (duration, magnitude, angle, onset speed), environment (speech ratio), and bimanual factors (ratio, overlap, and class). The total number of events for each subject was between 150 and 950 (median of 640 across subjects). Each distribution was normalized. These extracted features were used as inputs to the multiple regression models. Note that 3 pixels approximately equal 1 cm.

issue, we ignored data from the first 2 days post-surgery, removed electrodes with abnormal activity, and assessed movements across multiple days to avoid single-day bias. Another limitation is that the clinical video monitoring system includes only one camera, whose view can be obstructed by people and various objects throughout the day. We minimized obstruction effects by selecting movement events with high confidence scores in the event detection algorithm and manually reviewing all detected events to check if they were actual movements and not false positives, but using multiple cameras would extend body tracking to 3D in future studies. Finally, we confined our regression analysis to linear models. While studies have shown evidence of nonlinear relationships between electrocortical activity and behavior [19, 96], linear regression models provide easily interpretable results and allow straightforward assessments of individual feature contributions.

Our results underline the importance of studying naturalistic movements and understanding neural variability across multiple days. Our approach could be extended to other naturalistic movements and behaviors, such as grasping objects, sleep/wake transitions, and conversing with others. More broadly, our results have implications for developing novel brain-computer interfaces that can decode neural data across subjects in natural environments. For instance, movement data from many subjects could be combined to train decoders that generalize to new subjects with minimal re-training and are robust to a richer set of behavioral and environmental contexts. By publicly releas-

ing our curated dataset, we hope to spur further research that enhances our understanding of naturalistic behavior and informs the development of next-generation brain-computer interfaces.

## METHODS

### Subject information

We analyzed opportunistic clinical recordings from 12 subjects (8 males, 4 females) during their clinical epilepsy monitoring (conducted at Harborview Medical Center in Seattle, WA). Subjects were  $29.4 \pm 7.9$  years old at the time of recording (mean $\pm$ SD). Our study was approved by the University of Washington Institutional Review Board for the protection of human subjects. All subjects provided written informed consent.

We selected subjects who had ECoG electrode coverage near primary motor cortex, with either one  $8 \times 8$  or two  $4 \times 8$  electrode grids placed subdurally on the cortical surface. Additional electrodes were implanted on the cortical surface for some subjects, resulting in  $87.0 \pm 12.9$  total surface electrodes per subject (mean $\pm$ SD). In addition, five subjects had  $23.2 \pm 12.1$  intracortical depth electrodes (mean $\pm$ SD). Electrodes were implanted primarily within one hemisphere for each subject (5 right hemisphere, 7 left hemisphere). Single-subject electrode placement and recording duration information are given in Supplementary Table 2.

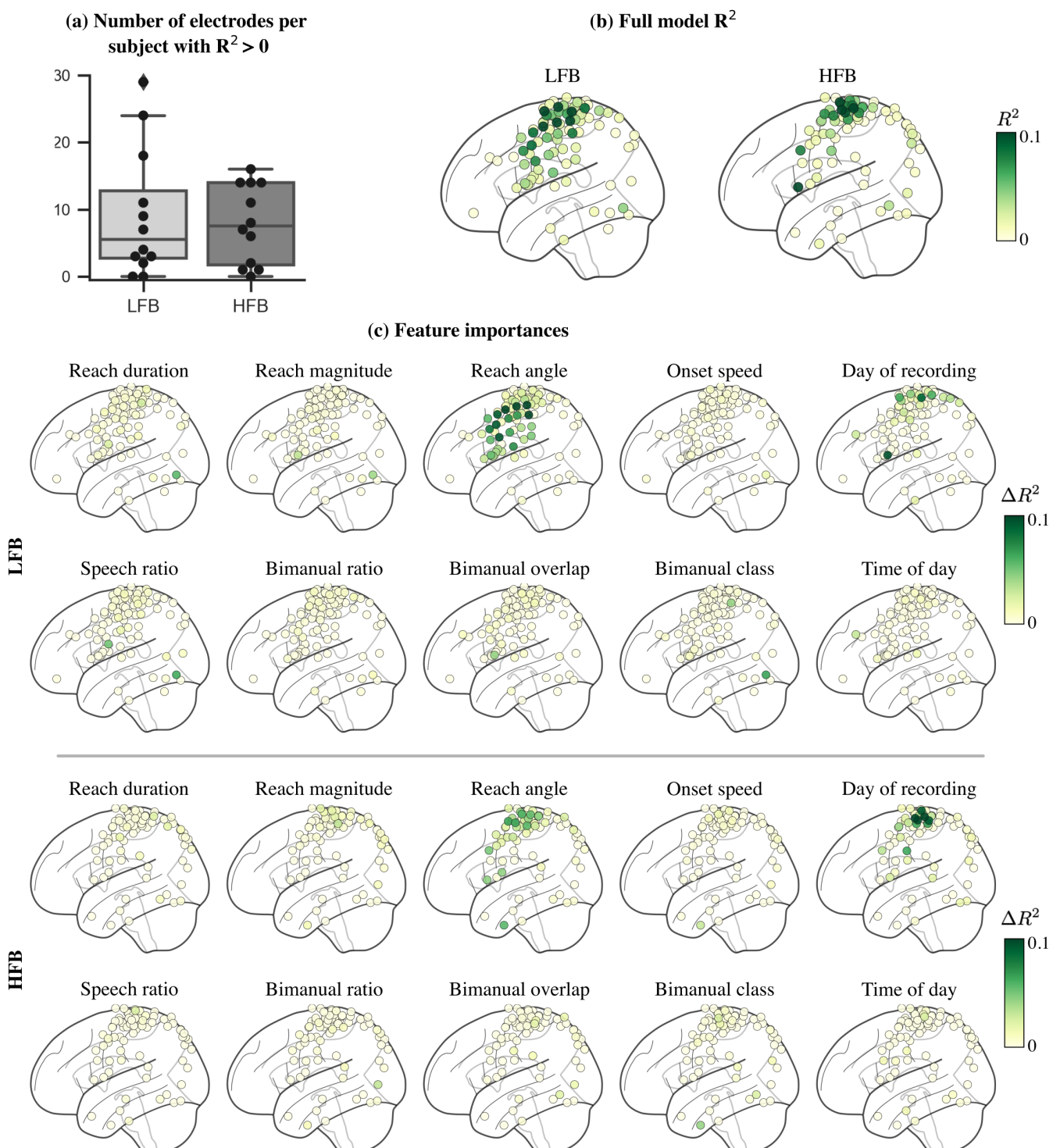


**Fig. 7: Event-by-event multiple regression models explain neural spectral power features using extracted behavioral and environmental features.** (a) The number of electrodes per subject with full model  $R^2 > 0$  is shown for low/high frequency band (LFB/HFB) spectral power. All  $R^2$  scores were computed on test data withheld from model fitting. (b) Models with the largest  $R^2$  scores were primarily located in sensorimotor areas. (c) Feature importance assesses how much the  $R^2$  on withheld data changed by shuffling a particular feature's training data. From this measure, we find that reach angle and day of recording were the most important features in this model. Only electrodes with positive full model  $R^2$  values are shown for (b)–(c).

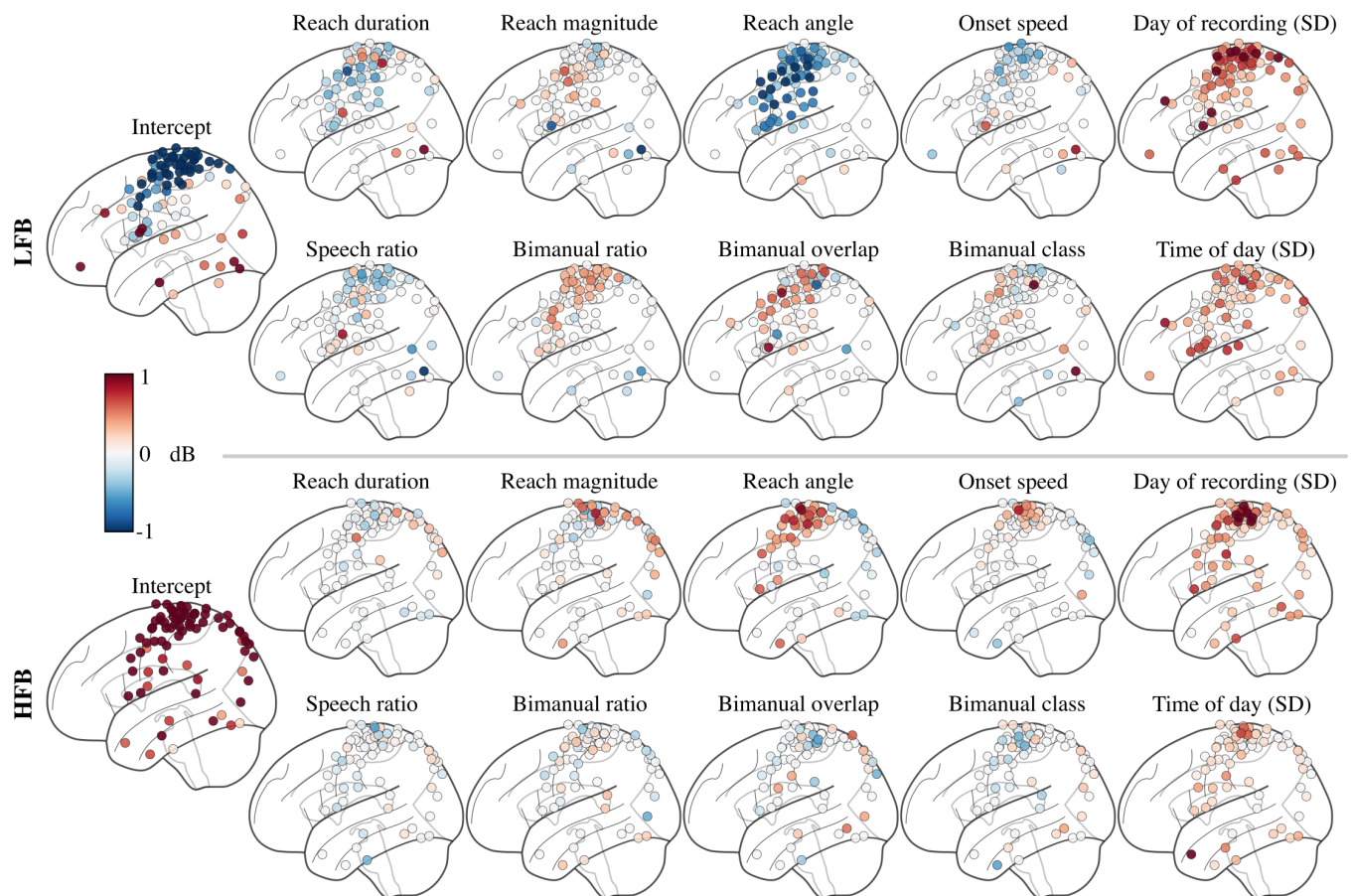


**Fig. 8: Coefficient weights of the multiple regression model, showing magnitude and direction for each model.** Weights are shown in units of spectral power. Day of recording and time of day features are shown as standard deviation (SD) of coefficient values across one-hot encoded variables. Both features have notable standard deviations, highlighting the importance of long-term temporal variability. Only electrodes with a positive  $R^2$  on withheld test data are plotted.

### Data collection

Subjects underwent 24-hour clinical monitoring, involving semi-continuous ECoG and audio/video recordings over  $7.4 \pm 2.2$  days per subject (mean $\pm$ SD). Some breaks occurred throughout monitoring (on average,  $8.3 \pm 3.2$  total breaks per subject, each lasting  $1.9 \pm 2.4$  hours [mean $\pm$ SD]). For all subjects, we restricted our analysis to days 3–7 following the electrode implantation surgery, in order to exclude potentially anomalous neural and behavioral activity immediately following electrode implantation surgery. For several subjects, some days were excluded due to corrupted or missing data files, as noted in Supplementary Table 2. During clinical monitoring, subjects were observed during a variety of typical everyday activities, such as eating, sleeping, watching television, and socializing while confined to a hospital bed. ECoG and video were initially sampled at 1000 Hz and 30 frames per second, respectively. Fig. 1 shows an example of the clinical monitoring setup, along with our data processing pipeline.

### ECoG data processing

We processed the raw ECoG data using custom MNE-Python scripts [97]. First, we removed DC drift by subtracting the median voltage of each electrode. Widespread, high-amplitude artifacts were then identified by abnormally high electrode-averaged absolute voltage ( $> 50$  interquartile range [IQR]). We set these artifacts to 0, along with all data within 2 seconds of each identified artifact. Removing such high-amplitude discontinuities minimizes subsequent filtering artifacts due to large, abrupt changes in the signal [98].

With data discontinuities removed, we band-pass filtered the data (1–200 Hz) and notch filtered to minimize line noise at 60 Hz and its harmonics. The data were then resampled to 500 Hz and re-referenced to the common median for each grid, strip, or depth electrode group. Electrodes with bad data were identified based on abnormal standard deviation ( $> 5$  IQR) or kurtosis ( $> 10$  IQR) compared to the median value across channels. This process resulted in the removal of  $4.9 \pm 4.9$  surface electrodes per subject and  $1.0 \pm 1.4$  depth electrodes for each of the 5 subjects with depth electrodes.

Electrode positions were localized using the Fieldtrip toolbox in Matlab [99, 100] to enable multi-subject analyses. This process involved co-registering preoperative MRI and postoperative CT scans, manually selecting electrodes in 3D space, and warping electrode positions into MNI space.

### Movement event identification and pruning

We performed markerless pose estimation on the raw video footage separately for each subject to determine wrist positions (Fig. 1a). First, for each subject, we manually annotated 1000 random video frames with the 2D positions of 9 keypoints: the subject's nose, ears, wrist, elbows, and shoulders (<https://tinyurl.com/human-annotation-tool>). Video frames were randomly selected across all days, with preference given to frames during active, daytime periods. These manually annotated frames were used to train a separate neural network model for each subject using DeepLabCut [60]. Each model was then applied to every video for that subject to generate estimated wrist trajectories.

Movement states were identified by applying a first-order autoregressive hidden semi-Markov model to each wrist trajectory. This state segmentation model classified the wrist trajectory into either a move or rest state. For this study, we focused on movements of the wrist contralateral to the implanted hemisphere. Contralateral wrist states were then discretized, and movement initiation events were identified at state transitions where 0.5 seconds of rest states are followed by 0.5 seconds of move states. See Singh et al. [61] for further methodological details.

After identifying movement initiation events, we coarsely labeled the video data manually (~3 minutes resolution) and excluded arm movements during sleep, unrelated experiments, and private times (as specified in our IRB protocol). In addition, we only retained movement events where (1) movement durations were between 0.5–4 seconds, (2) the confidence scores from DeepLabCut were  $> 0.4$ , indicating minimal marker occlusion, and (3) wrist movements followed a parabolic trajectory, as determined by a quadratic fit to the wrist's radial movement ( $R^2 > 0.6$ ). We found that this quadratic fit criteria eliminated many outliers with complex movement trajectories and improved the interpretability of our subsequent analyses. For each day of recording, we selected up to 200 events with the highest movement onset velocities. Finally, all movement initiation events were visually inspected, and events with occlusions or false positive movements were removed ( $17.8\% \pm 9.9\%$  of events [mean $\pm$ SD]).

### ECoG-event synchronization and segmentation

We used timestamps accompanying clinical recordings to synchronize movement initiation events with ECoG recordings and generated 10-second ECoG segments centered around each event. ECoG segments with missing data and large artifacts, such as line noise, were removed by computing log-transformed spectral power density for each segment and discarding segments with power below 0 dB or with abnormally high power at 115–125 Hz ( $> 3$  SD) compared to all segments. With these bad ECoG segments removed, we computed log-transformed, time-frequency spectral power using Morlet wavelets [101]. Power at each segment was then baseline-subtracted, using a baseline defined as 1.5–1 seconds before each movement initiation event.

### Projecting power into regions of interest

Because electrode placement was clinically motivated and varied greatly across subjects, we projected the spectral power computed at every electrode into common regions of interest defined by the AAL atlas [102]. Prior to projection, in order to combine all subjects, all right hemisphere electrode positions were flipped into the left hemisphere. Using EEGLAB and Matlab, we mapped from electrodes to small, predefined brain regions by positioning a three-dimensional Gaussian (2 cm full-width at half-maximum) centered at each electrode position and calculating the Gaussian's value at each small region [72, 103, 104]. The values across small regions were combined based on the AAL region boundaries, providing a mapping between each electrode and AAL region based on radial distance. We performed this projection procedure separately for each subject.

By summing the weights from these mappings across electrodes, we estimated the electrode density for each AAL region. We retained regions with an average electrode density  $> 3$  across subjects, resulting in 8 regions of interest (ROIs): middle frontal, precentral, postcentral, inferior parietal, supramarginal, superior temporal, middle temporal, and inferior temporal (Fig. 3). These 8 ROIs represent where most of the electrodes were located across subjects. We then normalized the weights for each ROI so that they summed to 1. These normalized weights were used to perform a weighted average of electrode-level spectral power for every ECoG segment, generating a spectral power estimate at each region of interest.

After projecting single-event spectral power onto regions of interest, we computed the median value across events separately for each subject and region. We then averaged the event-median spectral power across subjects to obtain group-level estimates for each region of interest. To mask spectral power patterns that were not significant, group-level spectral power for every frequency bin within each region of interest was then compared to a 2000-permutation bootstrap distribution generated from baseline time points. Non-significant differences from each bootstrap distribution were set to 0 ( $p > 0.05$ , two-sided bootstrap statistics, false discovery rate correction [105]).

#### *Comparison with visually instructed hand clenches*

For subjects 01–03, we compared our naturalistic arm movement results to instructed hand clenches recorded during a bedside experiment. For the controlled experiment, subjects were visually instructed to either clench their contralateral hand or stick out their tongue, followed by a brief rest period. We focused only on hand clench initiation events based on measurements recorded from a wired glove (CyberGlove II, CyberGlove Systems, San Jose, USA). Hand clench initiation events were manually selected based on distal index finger sensor voltage increases from baseline. We then computed baseline-subtracted spectral power using the same process as the naturalistic movements, except using a baseline of -1.1 to -0.6 seconds based on the average time between the stimulus cue and hand clench initiation. To compare electrocortical power during naturalistic and instructed movement initiation conditions, we averaged the spectral power over the first half second of movement initiation, divided into low frequency (8–32 Hz) and high frequency bands (76–100 Hz) used in previous research [4]. We compared this averaged power in each electrode to a 2000-permutation bootstrap distribution. Non-significant differences from each bootstrap distribution were set to 0 ( $p > 0.05$ , two-sided bootstrap statistics, false discovery rate correction). Additionally, we quantified inter-event spectral power variability by computing the median absolute deviation at each frequency band [106].

#### *Single-event behavioral metadata features*

We extracted multiple behavioral and environmental metadata features that quantify variations in movement parameters and environmental contexts. These features were later used as input variables for regression models of inter-event spectral power and can be divided into 4 categories.

#### *1) Timing features*

Day of recording and time of day for each movement initiation event are used to capture long-term variations in the neural response.

#### *2) Reach movement features*

To quantify differences in the detected movements, we defined a *reach* as the maximum radial displacement of the wrist marker during the detected move state compared to its position at each movement initiation event. These features included the duration and magnitude of each reach. We also computed the 2D reach angle and transformed angles at 90–270° to range from 90° to -90°, respectively. This transformation made the reach angle sensitive to vertical reach variations, with 90° for upward reaches and -90° for downward reaches. We also computed wrist marker radial speed during movement onset. Note that these movement features were based on the location of the video camera, which varied slightly across subjects and recording days.

#### *3) Environmental feature*

Based on results from the literature [23, 107], we were motivated to consider how environmental factors affect electrocortical power. Here, we examined the environmental factor of people talking during movement initiation. First, we cleaned the recorded audio signal using spectral noise gating (<https://www.audacityteam.org>), which performed 40 dB reduction on audio signal components that were similar to a selected noise period during rest. We then used the short-time Fourier transform to compute the spectral power from 370–900 Hz as a proxy for speech [108]. This power was divided by the total power at each time point, producing a ratio that is robust to broadband changes in the audio signal caused by noise. This speech ratio was smoothed using a 1st-order low-pass filter with 4.2 mHz cutoff to minimize the effects of transient changes in power due to noise. We then averaged this ratio from -1 to 1 seconds around each movement initiation event, generating a speech ratio feature that ranges from 0.0 to 1.0.

#### *4) Bimanual reach features*

While movement initiation event selection was based solely on contralateral wrist movement, the ipsilateral wrist can still move and may affect the electrocortical response. We quantified the relative magnitude of ipsilateral wrist movement by computing the ratio of the ipsilateral wrist reach magnitude to the sum of ipsilateral and contralateral reach magnitudes. In addition, we computed the temporal overlap between contralateral and ipsilateral move states over the duration of the entire contralateral wrist movement. Finally, we computed a binary feature that classified movements as either unimanual or bimanual based on the amount of temporal lag between contralateral and ipsilateral wrist movement onset. This feature was bimanual if a sequence of 4 consecutive move states of the ipsilateral wrist began either 1 second before contralateral wrist movement initiation or anytime during the contralateral wrist move state.

### Single-event spectral power linear regression

Using the 10 extracted behavioral features as independent variables, we fit a separate linear regression model to the spectral power at every electrode. While projecting onto cortical regions provided a useful visualization, we found that fitting regression models using projected power resulted in very poor model fits, likely due to electrodes with maximal power responses overlapping multiple regions and differing across subjects. All features were standardized prior to regression, with reach duration and reach magnitude features also being log-transformed. We categorized the two timing features using one-hot encoding based on day of recording and three 8-hour segments (12am–8am, 8am–4pm, 4pm–12am) for time of day because we do not expect linear long-term power changes within and across days. For the dependent variable, we averaged spectral power over the first half second of movement onset for subject-specific low/high frequency bands. These frequency bands were determined by visual inspection of maximal spectral power deviations, as shown in Fig. 4. We then randomly selected 90% of each subject’s total contralateral arm movement events as training data, while withholding the remaining 10% for testing model generalizability. For each model, we independently pruned input features using forward selection, retaining features that improved adjusted  $R^2$  for an ordinary least squares fit. This procedure helped minimize overfitting due to too many independent variables.

For training, we applied a multiple linear regression model for event-by-event spectral power patterns (shown schematically in Fig. 1i) defined as:

$$y_{jkf} = \beta_{0kf} + \sum_{i=1}^m \beta_{ikf} x_{ij} \quad (1)$$

where  $y_{jkf}$  is the spectral power for movement event  $j$  at electrode  $k$  averaged over frequency band  $f$ , during the first half second of movement initiation;  $x_{ij}$  is feature  $i$  at event  $j$ , and  $\beta_{ikf}$  is the coefficient for feature  $i$  at electrode  $k$  and frequency band  $f$  ( $\beta_{0kf}$  is the intercept term). We minimized the Huber norm during model fitting to improve model robustness to outliers.

After training, we performed model validation by computing the  $R^2$  on withheld data, referred to as the *full model*  $R^2$ . We also assessed the contribution of each behavioral feature independently by shuffling one feature, fitting a new model, and computing the  $R^2$  on the unshuffled, withheld data. This new  $R^2$  was subtracted from the full model  $R^2$  to obtain  $\Delta R^2$  as an estimate of that feature’s importance. We repeated this shuffling process and computation of  $\Delta R^2$  across all model features.

We computed independent regression models using forward selection, along with  $R^2$  and  $\Delta R^2$  scores, over all electrodes and for both low and high frequency bands. To minimize bias in our selection of training and testing data, we performed 200 random, independent train/test splits for every regression model, averaging the full model  $R^2$ ,  $\Delta R^2$ , and coefficients across all splits.

### DATA AVAILABILITY

Our curated dataset is publicly available without restriction, other than citation, through Figshare at <https://figshare.com/s/ef4ea24d67d16233f73d>. This public dataset contains synchronized neural and behavioral data that can be used to generate Figures 2b–c and Figures 3–8.

### CODE AVAILABILITY

Our data analysis code is publicly available without restriction, other than citation, on Github at [https://github.com/BruntonUWBio/naturalistic\\_arm\\_movements\\_ecog](https://github.com/BruntonUWBio/naturalistic_arm_movements_ecog). The code in this repository can be used in conjunction with our published dataset to reproduce all main findings and figures from our study. We ask that future studies building on our published data and code cite both this paper and [61].

### ACKNOWLEDGEMENTS

We thank John So for his extensive manual annotations of the video data; Kameron D. Harris, Nile Wilson, Kurt Weaver, and Leigh Weber for discussions and help with data collection and analysis; Jeneva Cronin, David Caldwell, James Wu, and Nile Wilson for collecting the experimental hand clench data; neurosurgeons Jeffrey G. Ojemann and Andrew Ko, as well as the excellent staff at Harborview Hospital Neurosurgery department, for their care of the patients during their monitoring. This research was supported by funding from the Defense Advanced Research Projects Agency (FA8750-18-2-0259), the National Science Foundation (1630178 and EEC-1028725), the Sloan Foundation, and the Washington Research Foundation.

### AUTHOR CONTRIBUTIONS

NXRW, RPNR, and BWB conceived of the study. SMP and SHS performed the data analysis. SMP, SHS, RPNR, and BWB interpreted the results. SMP and BWB wrote the manuscript. SMP, SHS, NXRW, RPNR, and BWB edited the final manuscript. RPNR and BWB acquired funding for the project.

### REFERENCES

- [1] Sober, S. J., Sponberg, S., Nemenman, I. & Ting, L. H. Millisecond spike timing codes for motor control. *Trends in Neurosciences* **41**, 644–648 (2018).
- [2] Kalaska, J. F. *From Intention to Action: Motor Cortex and the Control of Reaching Movements*, 139–178 (Springer US, Boston, MA, 2009).
- [3] Truccolo, W., Friehs, G. M., Donoghue, J. P. & Hochberg, L. R. Primary motor cortex tuning to intended movement kinematics in humans with tetraplegia. *The Journal of Neuroscience* **28**, 1163 (2008).
- [4] Miller, K. J. et al. Spectral changes in cortical surface potentials during motor movement. *Journal of Neuroscience* **27**, 2424–2432 (2007).

- [5] Umeda, T., Koizumi, M., Katakai, Y., Saito, R. & Seki, K. Decoding of muscle activity from the sensorimotor cortex in freely behaving monkeys. *NeuroImage* **197**, 512–526 (2019).
- [6] Nastase, S. A., Goldstein, A. & Hasson, U. Keep it real: rethinking the primacy of experimental control in cognitive neuroscience. *PsyArXiv* 1–12 (2020).
- [7] Dastjerdi, M., Ozker, M., Foster, B. L., Rangarajan, V. & Parvizi, J. Numerical processing in the human parietal cortex during experimental and natural conditions. *Nature Communications* **4**, 2528 (2013).
- [8] Jackson, A., Mavoori, J. & Fetz, E. E. Correlations between the same motor cortex cells and arm muscles during a trained task, free behavior, and natural sleep in the macaque monkey. *Journal of Neurophysiology* **97**, 360–374 (2007).
- [9] Wilson, N. R. *et al.* Cortical topography of error-related high-frequency potentials during erroneous control in a continuous control braincomputer interface. *Frontiers in Neuroscience* **13**, 502 (2019).
- [10] Omedes, J., Schwarz, A., Müller-Putz, G. R. & Montesano, L. Factors that affect error potentials during a grasping task: toward a hybrid natural movement decoding bci. *Journal of Neural Engineering* **15**, 046023 (2018).
- [11] Gilja, V. *et al.* Challenges and opportunities for next-generation intracortically based neural prostheses. *IEEE Transactions on Biomedical Engineering* **58**, 1891–1899 (2011).
- [12] Schalk, G. *et al.* Two-dimensional movement control using electrocorticographic signals in humans. *Journal of Neural Engineering* **5**, 75–84 (2008).
- [13] Taylor, D. M., Tillery, S. I. H. & Schwartz, A. B. Direct cortical control of 3d neuroprosthetic devices. *Science* **296**, 1829–1832. (2002).
- [14] Kubota, K. & Niki, H. Prefrontal cortical unit activity and delayed alternation performance in monkeys. *Journal of Neurophysiology* **34**, 337–347 (1971).
- [15] Fetz, E. E. Operant conditioning of cortical unit activity. *Science* **163**, 955 (1969).
- [16] Bizzi, E. Discharge of frontal eye field neurons during saccadic and following eye movements in unanesthetized monkeys. *Experimental Brain Research* **6**, 69–80 (1968).
- [17] Evarts, E. V. A technique for recording activity of subcortical neurons in moving animals. *Electroencephalography and Clinical Neurophysiology* **24**, 83–86 (1968).
- [18] Evarts, E. V. Relation of pyramidal tract activity to force exerted during voluntary movement. *Journal of Neurophysiology* **31**, 14–27 (1968).
- [19] David, S. V., Vinje, W. E. & Gallant, J. L. Natural stimulus statistics alter the receptive field structure of v1 neurons. *Journal of Neuroscience* **24**, 6991–7006. (2004).
- [20] Chandrasekaran, C., Trubanova, A., Stillittano, S., Caplier, A. & Ghazanfar, A. A. The natural statistics of audiovisual speech. *PLoS computational biology* **5**, e1000436–e1000436 (2009).
- [21] Chandrasekaran, C., Turesson, H. K., Brown, C. H. & Ghazanfar, A. A. The influence of natural scene dynamics on auditory cortical activity. *The Journal of Neuroscience* **30**, 13919 (2010).
- [22] Silbert, L. J., Honey, C. J., Simony, E., Poeppel, D. & Hasson, U. Coupled neural systems underlie the production and comprehension of naturalistic narrative speech. *Proceedings of the National Academy of Sciences* **111**, E4687–E4696. (2014).
- [23] Huth, A. G., de Heer, W. A., Griffiths, T. L., Theunissen, F. E. & Gallant, J. L. Natural speech reveals the semantic maps that tile human cerebral cortex. *Nature* **532**, 453–458 (2016).
- [24] Zuo, X. *et al.* Temporal integration of narrative information in a hippocampal amnesic patient. *bioRxiv* 713180 (2019).
- [25] Machens, C. K., Wehr, M. S. & Zador, A. M. Linearity of cortical receptive fields measured with natural sounds. *Journal of Neuroscience* **24**, 1089–1100. (2004).
- [26] Chang, L. & Tsao, D. Y. The code for facial identity in the primate brain. *Cell* **169**, 1013 – 1028.e14 (2017).
- [27] Scanlon, J. E. M., Townsend, K. A., Cormier, D. L., Kuziek, J. W. P. & Mathewson, K. E. Taking off the training wheels: Measuring auditory p3 during outdoor cycling using an active wet eeg system. *Brain Research* **1716**, 50–61 (2019).
- [28] Nordin, A. D., Hairston, W. D. & Ferris, D. P. Human electrocortical dynamics while stepping over obstacles. *Scientific Reports* **9**, 4693 (2019).
- [29] Ladouce, S., Donaldson, D. I., Dudchenko, P. A. & Letswaart, M. Understanding minds in real-world environments: Toward a mobile cognition approach. *Frontiers in human neuroscience* **10**, 694–694 (2017).
- [30] Zink, R., Hunyadi, B., Huffel, S. V. & Vos, M. D. Mobile eeg on the bike: disentangling attentional and physical contributions to auditory attention tasks. *Journal of Neural Engineering* **13**, 046017 (2016).
- [31] Gwin, J. T., Gramann, K., Makeig, S. & Ferris, D. P. Electrocortical activity is coupled to gait cycle phase during treadmill walking. *NeuroImage* **54**, 1289–1296 (2011).
- [32] Tsitsiklis, M. *et al.* Single-neuron representations of spatial targets in humans. *Current Biology* **30**, 245–253.e4 (2020).
- [33] Maidenbaum, S., Miller, J., Stein, J. M. & Jacobs, J. Grid-like hexadirectional modulation of human entorhinal theta oscillations. *Proceedings of the National Academy of Sciences* **115**, 10798 (2018).
- [34] Redcay, E. & Schilbach, L. Using second-person neuroscience to elucidate the mechanisms of social interaction. *Nature Reviews Neuroscience* **20**, 495–505 (2019).
- [35] Müller-Pinzler, L., Krach, S., Krämer, U. M. & Paulus, F. M. *The Social Neuroscience of Interpersonal Emotions*, 241–256 (Springer International Publishing, Cham, 2017).

- [36] Szymanski, C. *et al.* Teams on the same wavelength perform better: Inter-brain phase synchronization constitutes a neural substrate for social facilitation. *NeuroImage* **152**, 425–436 (2017).
- [37] Rice, K., Moraczewski, D. & Redcay, E. Perceived live interaction modulates the developing social brain. *Social cognitive and affective neuroscience* **11**, 1354–1362 (2016).
- [38] Anumanchipalli, G. K., Chartier, J. & Chang, E. F. Speech synthesis from neural decoding of spoken sentences. *Nature* **568**, 493–498 (2019).
- [39] Miller, K. J. A library of human electrocorticographic data and analyses. *Nature Human Behaviour* **3**, 1225–1235 (2019).
- [40] Takaura, K., Tsuchiya, N. & Fujii, N. Frequency-dependent spatiotemporal profiles of visual responses recorded with subdural ecog electrodes in awake monkeys: Differences between high- and low-frequency activity. *NeuroImage* **124**, 557 – 572 (2016).
- [41] Gunduz, A. *et al.* Neural correlates of visual-spatial attention in electrocorticographic signals in humans. *Frontiers in human neuroscience* **5**, 89–89 (2011).
- [42] Pistohl, T., Ball, T., Schulze-Bonhage, A., Aertsen, A. & Mehring, C. Prediction of arm movement trajectories from ecog-recordings in humans. *Journal of Neuroscience Methods* **167**, 105–114 (2008).
- [43] Ball, T., Kern, M., Mutschler, I., Aertsen, A. & Schulze-Bonhage, A. Signal quality of simultaneously recorded invasive and non-invasive eeg. *NeuroImage* **46**, 708–716 (2009).
- [44] Kanth, S. T. & Ray, S. Electrocorticogram (ecog) is highly informative in primate visual cortex. *The Journal of Neuroscience* **40**, 2430 (2020).
- [45] Schalk, G. & Leuthardt, E. C. Brain-computer interfaces using electrocorticographic signals. *IEEE Reviews in Biomedical Engineering* **4**, 140–154 (2011).
- [46] Jacobs, J. & Kahana, M. J. Direct brain recordings fuel advances in cognitive electrophysiology. *Trends in Cognitive Sciences* **14**, 162–171 (2010).
- [47] Talakoub, O. *et al.* Temporal alignment of electrocorticographic recordings for upper limb movement. *Frontiers in neuroscience* **8**, 431–431 (2015).
- [48] Pistohl, T., Schulze-Bonhage, A., Aertsen, A., Mehring, C. & Ball, T. Decoding natural grasp types from human ecog. *NeuroImage* **59**, 248–260 (2012).
- [49] Chung, J. W. *et al.* Beta-band oscillations in the supplementary motor cortex are modulated by levodopa and associated with functional activity in the basal ganglia. *NeuroImage: Clinical* **19**, 559–571 (2018).
- [50] Peterson, S. M. & Ferris, D. P. Differentiation in theta and beta electrocortical activity between visual and physical perturbations to walking and standing balance. *eneuro* **5**, ENEURO.0207–18.2018 (2018).
- [51] Tan, H. *et al.* Decoding gripping force based on local field potentials recorded from subthalamic nucleus in humans. *eLife* **5**, e19089 (2016).
- [52] Milekovic, T., Truccolo, W., Grün, S., Riehle, A. & Brochier, T. Local field potentials in primate motor cortex encode grasp kinetic parameters. *NeuroImage* **114**, 338–355 (2015).
- [53] Ofori, E., Coombes, S. A. & Vaillancourt, D. E. 3d cortical electrophysiology of ballistic upper limb movement in humans. *NeuroImage* **115**, 30–41 (2015).
- [54] Gabriel, P. G. *et al.* Neural correlates of unstructured motor behaviors. *Journal of Neural Engineering* **16**, 066026 (2019).
- [55] Alasfour, A. *et al.* Coarse behavioral context decoding. *Journal of Neural Engineering* **16**, 016021 (2019).
- [56] Wang, N. X., Farhadi, A., Rao, R. P. & Brunton, B. W. AJILE movement prediction: Multimodal deep learning for natural human neural recordings and video. In *Thirty-Second AAAI Conference on Artificial Intelligence* (2018).
- [57] Wang, N. X. R., Olson, J. D., Ojemann, J. G., Rao, R. P. N. & Brunton, B. W. Unsupervised Decoding of Long-Term, Naturalistic Human Neural Recordings with Automated Video and Audio Annotations. *Frontiers in Human Neuroscience* **10** (2016).
- [58] Vansteensel, M. J. *et al.* Task-free electrocorticography frequency mapping of the motor cortex. *Clinical Neurophysiology* **124**, 1169–1174 (2013).
- [59] Chao, Z., Nagasaka, Y. & Fujii, N. Long-term asynchronous decoding of arm motion using electrocorticographic signals in monkey. *Frontiers in Neuroengineering* **3**, 3 (2010).
- [60] Mathis, A. *et al.* DeepLabCut: Markerless pose estimation of user-defined body parts with deep learning. Tech. Rep., Nature Publishing Group (2018).
- [61] Singh, S. H., Peterson, S. M., Rao, R. P. N. & Brunton, B. W. Towards naturalistic human neuroscience and neuroengineering: behavior mining in long-term video and neural recordings. (2020).
- [62] Brunton, B. W. & Beyeler, M. Data-driven models in human neuroscience and neuroengineering. *Current Opinion in Neurobiology* **58**, 21–29 (2019).
- [63] Datta, S. R., Anderson, D. J., Branson, K., Perona, P. & Leifer, A. Computational neuroethology: A call to action. *Neuron* **104**, 11–24 (2019).
- [64] Berman, G. J. Measuring behavior across scales. *BMC Biology* **16**, 23 (2018).
- [65] Brown, A. X. & de Bivort, B. Ethology as a physical science. *Nature Physics* **14**, 653–657 (2018).
- [66] Anderson, D. J. & Perona, P. Toward a science of computational ethology. *Neuron* **84**, 18–31 (2014).
- [67] Huk, A., Bonnen, K. & He, B. J. Beyond trial-based paradigms: Continuous behavior, ongoing neural activity, and natural stimuli. *Journal of Neuroscience* **38**, 7551–7558. (2018).
- [68] Holdgraf, C. R. *et al.* Encoding and decoding models in cognitive electrophysiology. *Frontiers in Systems Neuroscience* **11**, 61 (2017).

- [69] van Gerven, M. A. J. A primer on encoding models in sensory neuroscience. *Journal of Mathematical Psychology* **76**, 172–183 (2017).
- [70] Portugues, R., Feierstein, C. E., Engert, F. & Orger, M. B. Whole-brain activity maps reveal stereotyped, distributed networks for visuomotor behavior. *Neuron* **81**, 1328–1343 (2014).
- [71] Naselaris, T., Kay, K. N., Nishimoto, S. & Gallant, J. L. Encoding and decoding in fmri. *NeuroImage* **56**, 400–410 (2011).
- [72] Bigdely-Shamlo, N., Mullen, T., Kreutz-Delgado, K. & Makeig, S. Measure projection analysis: a probabilistic approach to eeg source comparison and multi-subject inference. *NeuroImage* **72**, 287–303 (2013).
- [73] Skarpaas, T. L., Tcheng, T. K. & Morrell, M. J. Clinical and electrocorticographic response to antiepileptic drugs in patients treated with responsive stimulation. *Epilepsy & Behavior* **83**, 192–200 (2018).
- [74] Struck, A. F., Cole, A. J., Cash, S. S. & Westover, M. B. The number of seizures needed in the emu. *Epilepsia* **56**, 1753–1759 (2015).
- [75] Cronin, J. A. *et al.* Task-specific somatosensory feedback via cortical stimulation in humans. *IEEE transactions on haptics* **9**, 515–522 (2016).
- [76] Engel, A. K. & Fries, P. Beta-band oscillations—signalling the status quo? *Current Opinion in Neurobiology* **20**, 156–165 (2010).
- [77] Tam, W.-k., Wu, T., Zhao, Q., Keefer, E. & Yang, Z. Human motor decoding from neural signals: a review. *BMC Biomedical Engineering* **1**, 22 (2019).
- [78] Branco, M. P., de Boer, L. M., Ramsey, N. F. & Vansteensel, M. J. Encoding of kinetic and kinematic movement parameters in the sensorimotor cortex: A brain-computer interface perspective. *European Journal of Neuroscience* **50**, 2755–2772 (2019).
- [79] Branco, M. P. *et al.* High-frequency band temporal dynamics in response to a grasp force task. *Journal of Neural Engineering* **16**, 056009 (2019).
- [80] Manning, J. R., Jacobs, J., Fried, I. & Kahana, M. J. Broadband shifts in local field potential power spectra are correlated with single-neuron spiking in humans. *The Journal of Neuroscience* **29**, 13613 (2009).
- [81] Başar, E., Başar-Eroglu, C., Karakaş, S. & Schürmann, M. Gamma, alpha, delta, and theta oscillations govern cognitive processes. *International Journal of Psychophysiology* **39**, 241–248 (2001).
- [82] van Kerkoerle, T. *et al.* Alpha and gamma oscillations characterize feedback and feedforward processing in monkey visual cortex. *Proceedings of the National Academy of Sciences* **111**, 14332 (2014).
- [83] Miller, K. J., Zanos, S., Fetz, E. E., den Nijs, M. & Ojemann, J. G. Decoupling the cortical power spectrum reveals real-time representation of individual finger movements in humans. *The Journal of Neuroscience* **29**, 3132 (2009).
- [84] Harbourne, R. T. & Stergiou, N. Movement variability and the use of nonlinear tools: principles to guide physical therapist practice. *Physical therapy* **89**, 267–282 (2009).
- [85] Haar, S., Donchin, O. & Dinstein, I. Individual movement variability magnitudes are explained by cortical neural variability. *The Journal of Neuroscience* **37**, 9076 (2017).
- [86] Braun, D. A., Aertsen, A., Wolpert, D. M. & Mehring, C. Motor task variation induces structural learning. *Current biology : CB* **19**, 352–357 (2009).
- [87] Herzfeld, D. J. & Shadmehr, R. Motor variability is not noise, but grist for the learning mill. *Nature Neuroscience* **17**, 149–150 (2014).
- [88] Lisberger, S. G. & Medina, J. F. How and why neural and motor variation are related. *Current opinion in neurobiology* **33**, 110–116 (2015).
- [89] Musall, S., Kaufman, M. T., Juavinett, A. L., Gluf, S. & Churchland, A. K. Single-trial neural dynamics are dominated by richly varied movements. *Nature Neuroscience* **22**, 1677–1686 (2019).
- [90] Hu, K. *et al.* Decoding unconstrained arm movements in primates using high-density electrocorticography signals for brain-machine interface use. *Scientific Reports* **8**, 10583 (2018).
- [91] Georgopoulos, A., Schwartz, A. & Kettner, R. Neuronal population coding of movement direction. *Science* **233**, 1416–1419. (1986).
- [92] Melnik, A. *et al.* Systems, subjects, sessions: To what extent do these factors influence eeg data? *Frontiers in human neuroscience* **11**, 150–150 (2017).
- [93] Gliske, S. V. *et al.* Variability in the location of high frequency oscillations during prolonged intracranial eeg recordings. *Nature Communications* **9**, 2155 (2018).
- [94] Nurse, E. S. *et al.* Consistency of long-term subdural electrocorticography in humans. *IEEE Transactions on Biomedical Engineering* **65**, 344–352 (2018).
- [95] Gallego, J. A., Perich, M. G., Chowdhury, R. H., Solla, S. A. & Miller, L. E. Long-term stability of cortical population dynamics underlying consistent behavior. *Nature Neuroscience* (2020).
- [96] Ting, L. H. & McKay, J. L. Neuromechanics of muscle synergies for posture and movement. *Current Opinion in Neurobiology* **17**, 622–628 (2007).
- [97] Gramfort, A. *et al.* Meg and eeg data analysis with mne-python. *Frontiers in Neuroscience* **7**, 267 (2013).
- [98] Gibbs, J. W. Fourier's series. *Nature* **59**, 606–606 (1899).
- [99] Stolk, A. *et al.* Integrated analysis of anatomical and electrophysiological human intracranial data. *Nature Protocols* **13**, 1699–1723 (2018).
- [100] Oostenveld, R., Fries, P., Maris, E. & Schoffelen, J.-M. Fieldtrip: Open source software for advanced analysis of meg, eeg, and invasive electrophysiological data. *Computational intelligence and neuroscience* **2011**, 156869–156869 (2011).

- [101] Debnath, L. & Shah, F. A. *Wavelet Transforms and Their Applications* (Birkhäuser, 2015).
- [102] Tzourio-Mazoyer, N. *et al.* Automated anatomical labeling of activations in spm using a macroscopic anatomical parcellation of the mni mri single-subject brain. *NeuroImage* **15**, 273 – 289 (2002).
- [103] Delorme, A. & Makeig, S. Eeglab: an open source toolbox for analysis of single-trial eeg dynamics including independent component analysis. *Journal of Neuroscience Methods* **134**, 9 – 21 (2004).
- [104] Peterson, S. M., Rios, E. & Ferris, D. P. Transient visual perturbations boost short-term balance learning in virtual reality by modulating electrocortical activity. *Journal of neurophysiology* **120** 4, 1998–2010 (2018).
- [105] Benjamini, Y. & Hochberg, Y. Controlling the false discovery rate: A practical and powerful approach to multiple testing. *Journal of the Royal Statistical Society. Series B (Methodological)* **57**, 289–300 (1995).
- [106] Hoaglin, D. C., Mosteller, F. & (Editor), J. W. T. *Understanding Robust and Exploratory Data Analysis* (Wiley-Interscience, 2000), 1 edn.
- [107] Derix, J., Iljina, O., Schulze-Bonhage, A., Aertsen, A. & Ball, T. doctor or darling? decoding the communication partner from ecog of the anterior temporal lobe during non-experimental, real-life social interaction. *Frontiers in Human Neuroscience* **6**, 251 (2012).
- [108] Master, S., Biase, N. d., Pedrosa, V. & Chiari, B. M. The long-term average spectrum in research and in the clinical practice of speech therapists. *Pró-Fono Revista de Atualização Científica* **18**, 111 – 120 (2006).